Murata *et al. Journal of Wood Science* (2023) 69:25
https://doi.org/10.1186/s10086-023-02098-x

Journal of Wood Science

ORIGINAL ARTICLE

Open Access

Effect of thermal modification on the stress relaxation behavior and microstructure of the cell wall

Koji Murata[1*], Mayumi Utsumi[1,2], Tomoya Hirata[1,3] and Masashi Nakamura[1]

Abstract

The stress relaxation behavior and cell wall microstructure of sugi were evaluated after thermal modification. Stress relaxation is observed and has a broad relaxation spectrum, implying various relaxation mechanisms. The relaxation was analyzed using a stretched exponential function, namely, the Kohlrausch–Williams–Watts (KWW) function, which contains two parameters. Moreover, the structure of the amorphous phase in the cell wall was examined by small-angle X-ray scattering (SAXS) analysis using the mass fractal dimension. The variation in the relaxation spectrum reduced, and the specific relaxation time increased by thermal modification at 220 °C. The mass fractal dimension in SAXS increased owing to modification, indicating that the structure of the cell wall includes some defects between cellulose microfibrils. The mass fractal dimension was related to the relaxation parameter of the KWW function. Considering the change in crystallinity, the amorphous phase in the cell wall decomposed and condensed by thermal decomposition, which caused a longer relaxation time. Thus, the KWW function may be used to evaluate the stress relaxation behavior of wood, and the mass fractal dimension in SAXS can indicate the amorphous structure in the cell wall.

Keywords Stress relaxation, SAXS, WAXD, Stretched exponential function, KWW function, ThermoWood

Introduction

Thermal modification of wood has long been recognized as a potentially useful method to improve its dimensional stabilization and increase its decay resistance. Many studies have reported on the thermal modification of wood [1–7], which is the most advanced commercial wood modification process. For example, ThermoWood®, which is the registered trademark owned by the Finnish ThermoWood Association, is one of the most popular thermally modified wood products. ThermoWood is thermally processed in the presence of steam, which acts as a blanket to limit the oxidative degradation of wood. Additional chemical reactions also occur as a result of the presence of moisture. The heating of wood in the presence of water or steam results in accelerated formation of organic acids (primarily acetic acid) that catalyze the hydrolysis of hemicellulose [8]. The amorphous region of the wood cell wall consists of hemicellulose and lignin, and the rheological behavior, such as stress relaxation, partly depends on the properties of the amorphous region.

Multiple-component materials, such as wood with crystalline amorphous materials, differ from synthetic amorphous polymers and have a non-characteristic spectrum that is generally a broad peak [9]. Therefore, various factors related to the relaxation behavior of wood have received little attention with regard to the relaxation spectrum. However, new approaches for analyzing the relaxation spectrum

*Correspondence:
Koji Murata
murata.koji.4e@kyoto-u.ac.jp
[1] Graduate School of Agriculture, Kyoto University, Sakyo, Kyoto 606-8502, Japan
[2] Present Address: Ministry of the Environment, Government of Japan, Chiyoda-ku, Tokyo 100-8975, Japan
[3] Present Address: Accenture Japan Ltd, Kita-ku, Osaka 530-0005, Japan

Springer Open

© The Author(s) 2023. **Open Access** This article is licensed under a Creative Commons Attribution 4.0 International License, which permits use, sharing, adaptation, distribution and reproduction in any medium or format, as long as you give appropriate credit to the original author(s) and the source, provide a link to the Creative Commons licence, and indicate if changes were made. The images or other third party material in this article are included in the article's Creative Commons licence, unless indicated otherwise in a credit line to the material. If material is not included in the article's Creative Commons licence and your intended use is not permitted by statutory regulation or exceeds the permitted use, you will need to obtain permission directly from the copyright holder. To view a copy of this licence, visit http://creativecommons.org/licenses/by/4.0/.

are similar to the numerical calculation method of the Fourier transform [10]. The Kohlrausch–Williams–Watts (KWW) function is also one of the new approaches suitable for studying materials such as wood because the relaxation characteristics are controlled by two parameters [11].

The cell wall of wood consists of crystalline cellulose and a matrix composed of hemicellulose and lignin. Crystalline cellulose, also known as cellulose microfibrils (CMFs), is surrounded by the matrix in the cell wall. In a previous study, crystalline cellulose was observed using wide-angle X-ray diffraction (WAXD) and small-angle X-ray scattering (SAXS) [12]. A cylindrical model of the average crystalline regions in an elementary cellulose fibril was proposed for the X-ray method. In SAXS, the X-rays scattered owing to the differences in the electron density of matter are measured, and information about the nanostructure can be obtained from the scattering profile. To observe a large structure of several tens to several hundreds of nanometers, a device with excellent small-angle resolution is required, which is achieved using a synchrotron radiation system.

In this study, we evaluated the stress relaxation of wood that was thermally modified in steam atmosphere using the KWW function with two parameters. In addition, the crystalline and amorphous structures of thermally modified wood were evaluated by X-ray analysis, and the relationship between the stress relaxation mechanism and the structure of the cell wall was examined.

Materials and methods

Theory

An external stimulus such as deformation applied to a viscoelastic body generates stress as a response. When the external force stimulus is kept constant (ε_c), the stress (σ) decreases depending on time (t), which is called stress relaxation. For the Maxwell model, the relaxation elastic modulus ($E(t)$), is expressed by Eq. (1), where $E(0)$ denotes the instantaneous elastic modulus immediately after deformation ($t=0$):

$$E(t) = \frac{\sigma(t)}{\varepsilon_c} = E(0)\exp\left(-\frac{t}{\tau}\right), \tag{1}$$

where τ denotes the relaxation time. Wood is considered a multicomponent viscoelastic body, and according to the linear viscoelastic theory, $E(t)$ is expressed by the following equation based on Boltzmann's superposition theory [Eq. (2)].

$$\begin{aligned} E(t) &= \int_0^\infty \Phi(\tau)\exp\left(-\frac{t}{\tau}\right)d\tau \\ &= \int_{-\infty}^\infty H(\ln\tau)\exp\left(-\frac{t}{\tau}\right)d\ln\tau. \end{aligned} \tag{2}$$

Here $\Phi(\tau)$ and $H(\ln\tau)$ are the relaxation spectra. The characteristic properties of the stress relaxation of wood is explained using $\Phi(\tau)$ or $H(\ln\tau)$. The stretched exponential function (KWW function) has been used to analyze the relaxation behavior of various materials, such as dielectric relaxation [13–15]. Nakao and Nakano [11] explained the application of the KWW function, which uses only two parameters in the analysis of the stress relaxation of wood. Using the KWW function, $E(t)$ can be expressed as shown in Eq. (3):

$$E(t) = E(0)\exp\left[-\left(\frac{t}{\tau_0}\right)^\beta\right], \tag{3}$$

where β is the "stretching parameter" that describes the distribution of relaxation time, and τ_0 is the characteristic relaxation time. Rescaling Eq. (3) in logarithmic form, and transposing the terms, we obtain Eq. (4):

$$\ln[E(0)] - \ln[E(t)] = \left(\frac{t}{\tau_0}\right)^\beta. \tag{4}$$

Furthermore, the logarithm of both sides in Eq. (4) yields a linear function of time, $\ln(t)$, in Eq. (5):

$$\ln\left\{\ln[E(0)] - \ln[E(t)]\right\} = \beta\ln t - \beta\ln(\tau_0). \tag{5}$$

Thermal modification

Kiln-dry lumber of sugi (*Cryptomeria japonica*) was used as a common material. Thermal modification was

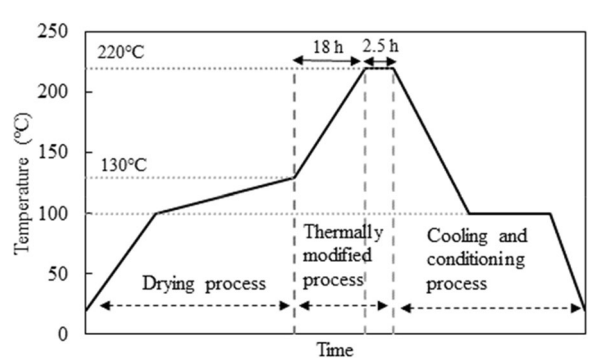

Fig. 1 Schematic of thermal modification (220 °C process)

performed in a steam atmosphere, according to the ThermoWood process (Fig. 1). First, the kiln-dried lumber was gradually dried until the equilibrium moisture content reached approximately 0% (drying process). Next, it was heated at a rising rate of 5 °C/h, and then heated at 220 °C and 237.5 °C for 2.5 h and 5 h, respectively (thermally modified process). Finally, after heat treatment, the temperature was gradually lowered to adjust the moisture content to match the indoor humidity (cooling/conditioning process). The thermal modifications were carried out according the ThermoWood process (D2, D1+++) used in our partner's mill, where D2 (220 °C) is standard grade in the mill, and D1+++ (237.5 °C) is the best grade for decay resistance and dimensional stability. According to the Thermowood Handbook [16], bending strength and elastic modulus decrease linearly from 200 to 240 °C in thermally modification under a steam atmosphere. On the other hand, when thermally modified at 230 °C, the biological durability is remarkably improved. Also, as a result of the heat treatment process, the structure of wood cells is re-formed.

Measurement of cell wall density

The density of the wood was measured using the water displacement method [15]. Five small wood specimens [10 mm (T) × 10 mm (R) × 3 mm (L)] were prepared for each type (control, 220 °C, and 237.5 °C) was 5. First, the oven-dried weight was obtained, and the dried wood was impregnated with water in a vacuum chamber. The cycle from vacuum to normal pressure was repeated several times. After sinking the specimen in water, the weights were measured in water under the influence of buoyancy. The density of the wood was calculated using Eq. (6):

$$\rho = \frac{m}{m - m'}\rho_{\mathrm{w}}, \tag{6}$$

where m and m' are the oven-dried weight and weight in water, respectively, and ρ_{w} is the density of water (0.99704 g/cm^3).

Stress relaxation in tensile test

Specimens for the tensile test were prepared from the control and thermally modified wood. The dimensions were 70 mm (T) × 15 mm (R) × 5 mm (L). Five specimens were prepared for each type. The tensile tests were performed using a load testing machine (ADT-AV10K1S5, Shimadzu), where the distance between the clamps was 35 mm. A tensile displacement of 0.4 mm was applied in the tangential direction, and the distance was maintained for almost 20 h. The experiments were performed in the same room in which the specimens have been adjusted to equilibrium moisture content. The strain on the specimen was measured using a strain gauge (gauge length of 10 mm), and the tensile load was divided by the cross-sectional area to obtain the tensile stress in the specimen. The relaxation elastic modulus was calculated using the constant strain and time-dependent stress. The stretching parameter (β) and specific relaxation time (τ_0) were obtained using the KWW function (Eq. (5)).

Analysis using WAXD

The specimen for WAXD, which was 30 mm (L) × 20 mm (R) × 1 mm (T), was conditioned at a temperature of 20 °C and RH of 60%. WAXD was performed using a X-ray diffractometer (RINT2200, Rigaku) with an acceleration voltage and acceleration current of 40 kV and 30 mA, respectively. X-rays (CuKα 0.1541841 nm) were irradiated in the tangential direction of the specimen and scanned using the reflection method. The measurement range was 5°–40°, with a step width of 0.02° and sampling speed of 1°/min. To obtain information about the structure of the cell wall, the diffraction signal was isolated into distributions $I_{\mathrm{G}}(2\theta)$ of each crystal using Eq. 7 [17]:

$$I_{\mathrm{G}}(2\theta) = I_{\max} \cdot \exp\left\{-4(\ln 2) \cdot \left(\frac{2\theta - 2\theta_{\max}}{B}\right)^2\right\}. \tag{7}$$

Here, $I_{\max}$, $2\theta_{\max}$, and B denote the maximum peak of the distribution, deflection angle of the maximum peak, and full width at half maximum. The diffraction distributions were assumed to comprise three crystal planes, namely, (110), (200), and (004), one noncrystal diffraction, and a baseline. To fit the distribution function, the parameters were optimized by the nonlinear least-squares method using the solver function of Microsoft Excel®.

The isolated diffraction curve was used to obtain the Scherrer width D of the crystal and crystallinity C_{r} using Eqs. (8) and (9), respectively:

$$D = \frac{K\lambda}{B\cos\theta_{200}}, \tag{8}$$

$$C_{\mathrm{r}} = \frac{S_{\mathrm{cr}}}{S_{\mathrm{cr}} + S_{\mathrm{nc}}}, \tag{9}$$

where K is a constant (0.94), λ is the X-ray wavelength (0.154 nm), S_{cr} is the sum of the integrated intensities of the crystal peaks in each plane, and S_{nc} is the integrated intensity of the amorphous peaks.

Analysis using SAXS

The specimen for SAXS, which was 30 mm (L) × 20 mm (R) × 5 mm (T), was prepared and conditioned at a temperature of 20 °C and RH of 60%. SAXS was performed in the beam line BL40B2 of the synchrotron radiation facility SPring-8 to obtain two-dimensional X-ray scattering profiles. The quarter-sawn specimens were irradiated with X-rays of 1 Å wavelength, and the detector (PILATUS3S 2 M, DECTRIS) was placed 4 m away from the specimen. The scattered signal was captured once per specimen for an exposure time of 1 s. The intensity profile in each direction was calculated from the two-dimensional scattering signal using PyFAI (open-source Python library). The maximum intensity was observed in the equatorial direction (approximately 0°). To obtain a one-dimensional scattering profile in the radial direction of the detector image, the signal patterns were integrated azimuthally on 25° wide sectors around the equatorial maximum direction, following the method described in [18].

The scattering functions were plotted in the log $I = f(q^2)$ representation. To estimate the size of particles or pores, the Guinier radius R_g was determined in the first slope of the scattering curve from the Guinier function [19, 20]. The diameter d of the particles was calculated using Eqs. (10) and (11):

$$\ln(I) = -\frac{R_g^2}{3}q^2 + \ln(I_0), \tag{10}$$

$$d = \frac{2\sqrt{5}}{3}R_g. \tag{11}$$

A fractal is a figure whose parts and whole are self-similar, and the fractal dimension is used to quantitatively evaluate the complexity of a self-similar figure. The nanostructure of wood is also considered to exhibit self-similarity, and structural analysis has been performed using the mass fractal dimension (D_m) and surface fractal dimension (D_s) which indicate self-similarity of matrix structure and smoothness of the particle or pore surface, respectively [21, 22]. Equations (12) and (13) explain the relationship between the fractal dimensions D_m and D_s and the scattering intensity of SAXS, respectively:

$$I(q) \propto q^{-D_m}, \tag{12}$$

$$I(q) \propto q^{-(6-D_s)}. \tag{13}$$

The fractal dimensions satisfy the conditions $2 < D_s < 3$ and $1 < D_m < 3$. The fractal dimensions were obtained by constructing a log–log plot of Eq. (12) or Eq. (13).

Results and discussion

Density and equilibrium moisture content

Table 1 lists the density and moisture content of the specimens conditioned for more than a month under standard atmosphere (20 °C, 65% RH) after thermal modification. The moisture content decreased with increasing modification temperature. Figure 2, which shows the density of the cell wall measured using the water displacement method, indicates that thermal modification also reduces the density of the cell wall slightly, but no statistically significant difference was found although the apparent densities of whole specimen did change clearly.

It is difficult to find the previous studies about chemical changes of wood by thermally modification over 220 °C under steam atmosphere. Sun et al. [23] investigated chemical composition and hygroscopicity of Eucalyptus specimen which were thermally modified in vacuum oven at 160–240 °C under negative pressure (−0.02 to −0.08 MPa) in order to avoid from effect of oxygen similar under steam atmosphere. They found that thermal modification made holocellulose and alpha-cellulose contents decreased, and lignin and extractives contents relatively increased. Moreover, the hygroscopicity was related to the relative content of lignin, the degradation of carbonyl groups in xylan and the loss of carbonyl group. Hieralta et al. [24] examined the cell wall microporosity of thermally modified wood in steam using NMR spectroscopy. They showed that the size or distribution of

Table 1 Density and moisture content of the specimens

	Control	220 °C	237.5 °C
Density (kg/m^3)	361	313	282
Moisture content (%)	11.9	4.4	3.5

"Control" indicates the specimen without thermal modification

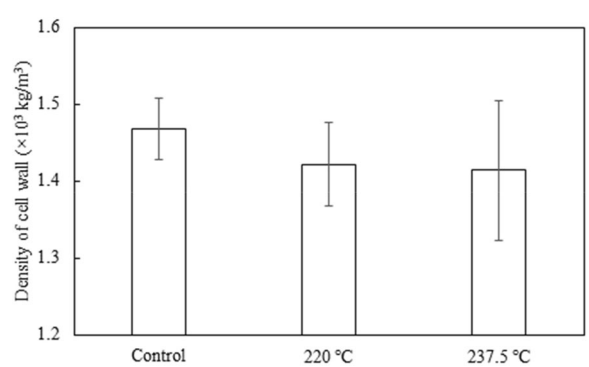

Fig. 2 Effect of thermal modification on the density of the cell wall. The error bars indicate the standard deviation

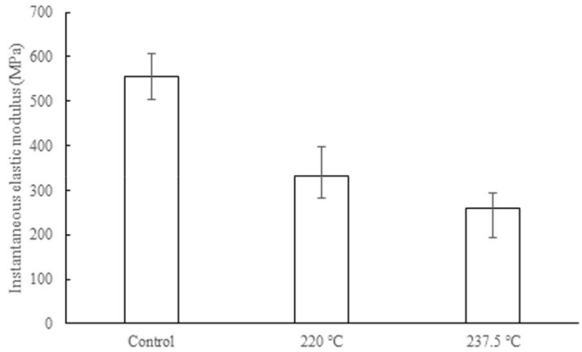

Fig. 3 Change of the instantaneous elastic modulus. The error bars indicate the standard deviation

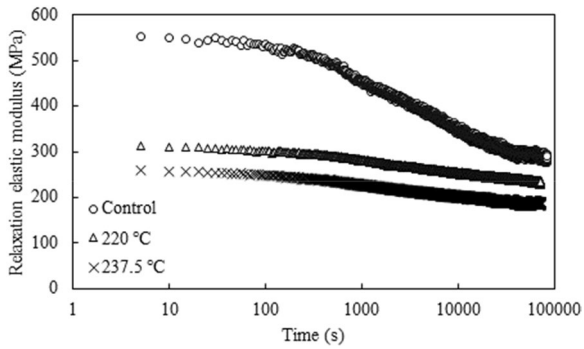

Fig. 4 Examples of the relaxation elastic modulus

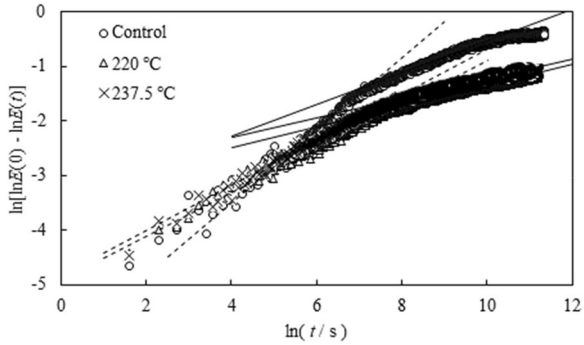

Fig. 5 Relationship between ln(t) and ln(ln$E$(0) − ln$E$(t)) according to the KWW function

cell wall micropores significantly increased at the temperatures higher than 180 °C, and the average size of the micropores was tens of nanometers. The changes in equilibrium moisture content may be attributed to the increase in micropores and the changes of chemical components.

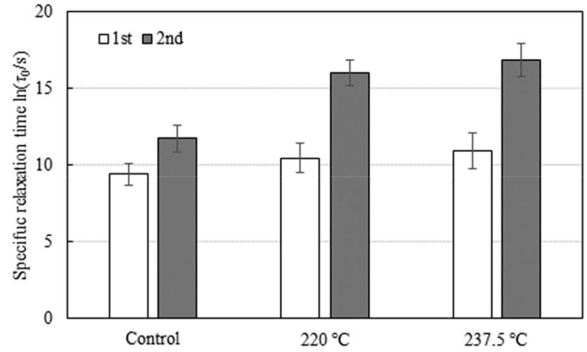

Fig. 6 Change of the specific relaxation time ln(τ_0). The error bars indicate the standard deviations

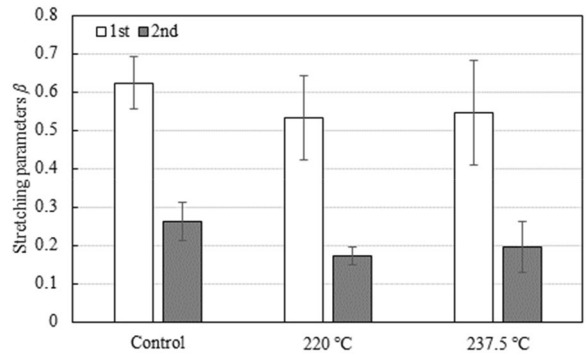

Fig. 7 Change of the stretching parameter β. The error bars indicate the standard deviations

Stress relaxation

The instantaneous elastic modulus (initial elastic modulus) is shown in Fig. 3. Thermal modification reduced the instantaneous elastic modulus, which is related to the physical properties of the cellulose crystals and amorphous components. An example of the change in relaxation elastic modulus over time is presented in Fig. 4, which shows that the thermal modification reduces the amount of relaxation. Next, Fig. 5 shows the relationship between the elapsed time ln(t) and relaxation modulus ln [ln$E$(0) − ln$E$(t)] according to Eq. (5), which is obtained by applying the KWW function: A two linear regions appear in the first stage from 150 s (ln(t) = 5) to 1100 s (ln(t) = 7) and in the second stage from 2980 s (ln(t) = 8) to 22,000 s (ln(t) = 10) after the beginning of the test, indicating that the KWW function is available.

Figures 6 and 7 show the changes in the two parameters obtained from the KWW function in Eq. (5). The first and second liner regions are called 1st and 2nd, respectively. The specific relaxation time τ_0 increases

with thermal modification, while the stretching parameters decrease in the first and second stage at the temperature of 220 °C and 237.5 °C. The difference between at the temperatures of 220 °C and 237.5 °C was slight. The differences of relaxation times may be related to free volume in rheology. The free volume in first stage was smaller than second stage, and the free volume became larger by thermal treatment. The stretching parameter β shows the distribution or spread of the peak at the relaxation time τ_0. This indicates that thermal modification narrows the distribution of the relaxation mechanism. Micropores and aggregation are created by thermal modification. The properties of the amorphous component contribute to the stress relaxation mechanism [11], and the micropores in the amorphous region homogenize the stress relaxation mechanism. A change in the relaxation mechanism, namely, the disappearance of a relatively low-molecular-weight structure, may result in a longer characteristic relaxation time. Kubovský et al. [25] evaluated chemical changes at thermal modification of oak wood in the temperature of 160, 180 and 210 °C. Using FTIR spectroscopy, they knew that the higher temperature caused the condensation reactions and the increase of molecular weight of lignin. Degradation of hemicelluloses included the cleavage of the polysaccharide chains and crosslinking reactions at 210 °C. Crosslinking in thermally degraded celluloses can take two form of hydrogen bonding between adjacent chains, or formation of covalent bridges. The higher thermally modified, the more crosslinking of wood components happened. Much crosslinking makes the molecular weight larger and the specific relaxation time longer.

WAXD

Table 2 shows the changes in crystallinity and crystal size (Scherrer width) owing to thermal modification. The crystal size is approximately 3 nm, and is identified as cellulose microfibril [12]. The thermal modification at 220 °C increased the crystal size, while that at 237.5 °C it changed slightly from at 220 °C. In addition, although the crystallinity slightly increased with the treatment at 220 °C, it decreased with the treatment at 237.5 °C. Bhuiyan et al. [26] explained that the crystal size increases owing to the reorientation of the cellulose crystal, which increases the crystallinity in the early stages of modification, and the increase in crystal size is related to the decrease in the amorphous regions. This is affected by the change in the degree of crystallinity, and when the relative crystallinity exceeds 1.1, the thermal decomposition of cellulose begins and the relative crystallinity decreases. Figure 8 shows the relationship between the relative crystallinity and relative crystal size. The results of this study are consistent with this finding. Sun et al. [23] showed that chemical analysis of the wood component of untreated and heat-treated eucalypt wood at 160–240 °C. The ratio of alpha-cellulose in holocellulose changed slightly up to 220 °C, while it decreased from 220 to 240 °C. Klason lignin changed slightly to 220 °C,

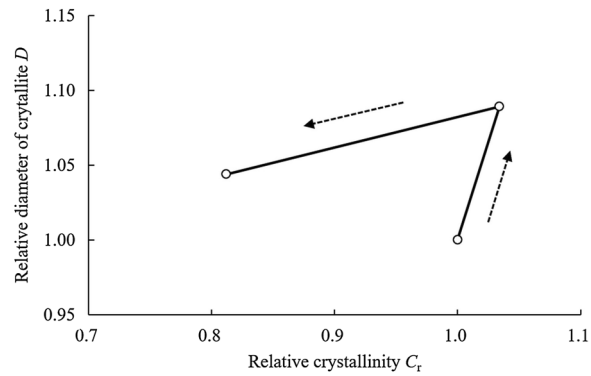

Fig. 8 Relationship between the relative crystallinity C_r and relative diameter of the crystal D

Table 2 Crystal size and crystallinity of thermally modified specimen obtained by WAXD

Thermal modification condition	Control	220 °C	237.5 °C
Crystal size D (nm)			
Average	3.03	3.30	3.17
Max.	3.06	3.32	3.19
Min.	2.97	3.28	3.15
Crystallinity C_r (%)			
Average	40.7	42.1	33.1
Max.	41.1	42.6	35.4
Min.	40.1	41.6	29.0

Table 3 Diameter of particle and fractal dimension obtained by SAXS

	Control	220 °C	237.5 °C
Diameter of particle d (nm)			
Average	2.62	3.39	3.19
Max.	3.11	3.21	3.11
Min.	2.15	3.65	3.24
Surface fractal dimension D_s			
Average	1.87	1.88	1.74
Max.	2.01	2.07	1.74
Min.	1.74	1.75	1.73
Mass fractal dimension D_m			
Average	2.28	2.61	2.63
Max.	2.59	2.69	2.65
Min.	2.07	2.55	2.59

while it increased from 220 to 240 °C. Alcohol–benzene extractives imply the degradation of polysaccharides, and the content of it changed slightly up to 220 °C, while it increased from 220 to 240 °C like Klason lignin. Lignin is the most thermally stable constituent in wood chemical components. In this study, the thermal modification at 220 °C caused expansion of cellulose crystal and degradation of polysaccharides at the same time. On the other hand, at 237.5 °C the size of cellulose crystal did not change, and polysaccharides were rapidly thermally decomposed.

SAXS

Table 3 shows the particle diameters and fractal dimensions obtained by SAXS. The change in the particle diameter d obtained from the Guinier equation [Eqs. (10) and (11)], which denotes the relationship between the diameter d and treatment temperature. Although the absolute values are slightly different, the results are similar to those obtained with WAXD. The mass fractal dimension D_m and surface fractal dimension D_s were obtained in the ranges of $-3.5 < \ln(q) < -1.5$ and $0 < \ln(q) < 0.5$, respectively, by SAXS, which were liner regions in the graphs of $\ln(q)$ and $\ln(I)$ The surface fractal dimension was obtained on the small-angle side ($q < 0.22$ nm^{-1}). Jakob et al. [27] found that X-ray scattering profiles remained unchanged at moisture contents below 14% and changed above 27%, where the scattering reflected the interface between free water and surface in the cell lumen. The smoother surface in the lumen lowered D_s owing to the thermal modification. However, some of D_s in this test may not have incorrect because they were less than 2.

Penttilä et al. [28] observed birch sawdust using SAXS analysis and found that the mass fractal dimension before drying was 2.79, but the dimension decreased after freeze-drying. It was explained that this is due to the presence of water molecules between cellulose microfibrils. In this study, thermal modification increased the mass fractal dimension because pyrolysis causes defects in the matrix structure between cellulose microfibrils (Table 3). The mass fractal dimension at 220 °C increased compering with the control, and it may show the condensation reactions of lignin, and the cleavage of the polysaccharide chains and the crosslinking reactions. These results were consistent with those of the WAXD study. Figure 9 shows the relationship between the relative β or relative $\ln(\tau)$ and D_m. The parameters of stress relaxation are related to mass fractal dimension, namely, the physical properties of the amorphous component. The mass fractal dimension D_m is correlated with the parameters and may reflect the state of the amorphous component.

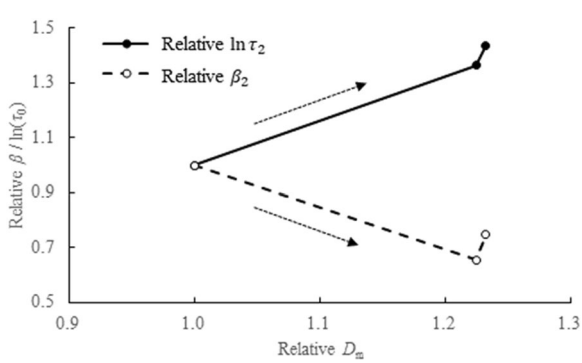

Fig. 9 Relationship between the relative D_m and relative β or relative $\ln(\tau_0)$ in second relaxation

In this study, we compared thermal modification at 220 °C and 237.5 °C for dimensional stability and durability. Although there was a difference in crystallinity, there was no difference in relaxation behavior, which is thought to be related to the amorphous structure. Next, it will be necessary to find other factors related to dimensional stability and durability.

Conclusion

Wood specimens (sugi) were heated in steam at 220 °C and 237.5 °C, and the changes in the cell wall density and stress relaxation parameters were evaluated according to thermal modification. To evaluate the relaxation mechanism and relaxation time, the stretched exponential function (KWW) was applied to the relaxation elastic modulus, which was related to the physical behavior of the amorphous component. In addition, the crystal structure and amorphous components were observed by WAXD and SAXS. The conclusions are summarized as follows:

1. The stress relaxation behavior of the thermally modified wood was analyzed using the KWW function. Two relaxation mechanisms appeared according to KWW function. The variation in the relaxation mechanism reduced, and the specific relaxation time increased owing to thermal modification in the tensile test under the standard condition of 20 °C and 65% RH. There was no difference in relaxation behavior, which is thought to be related to the amorphous structure. Next, it will be necessary to find other factors related to dimensional stability and durability.
2. According to the WAXD analysis, the crystal size increased and crystallinity of cellulose reduced upon treatment at 220 °C. However, upon the modification at 237.5 °C, the crystal size did not change and the crystallinity reduced. The crystallinity decreased owing to pyrolysis, and the reorientation of cellulose crystal increased its size by modification at 220 °C.

3. According to SAXS analysis, the mass fractal dimension increased at 220 °C and 237.5 °C. Considering the stress relaxation parameters, the mass fractal dimension of X-ray scattering explains the structure of the amorphous component in the wood cell wall.

It was concluded that the KWW function is suitable for evaluating the relaxation behavior of the amorphous component in the wood cell wall, while the mass fractal dimension in SAXS can be used to explain the structure of the amorphous component.

List of symbols

KWW	Kohlrausch–Williams–Watts
SAXS	Small-angle X-ray scattering
WAXD	Wide-angle X-ray diffraction
ε_c	Constant strain in stress relaxation test
σ	Stress in relaxation test
t	Time
E	Relaxation elastic modulus
τ	Relaxation time
$\Phi(\tau)$, $H(\ln\tau)$	Relaxation spectra
β	Stretching parameter in the KWW function
τ_0	Specific relaxation time
ρ	Density of cell wall
ρ_w	Density of water
m	Oven-dried weight
m'	Weight in water
2θ	Deflection angle in WAXD
I	Intensity of the X-ray signal
D	Scherrer width of the crystal
B	Full width of half maximum in X-ray signal
K	Constant of the Scherrer equation.
λ	X-ray wavelength
S_{cr}	Sum of the integrated intensities of the crystal peaks on each plane
S_{nc}	Integrated intensity of amorphous peaks.
C_r	Crystallinity
q	Scattering vector
R_g	Guinier radius
d	Diameter of particles from the Guinier radius
D_m	Mass fractal dimension in SAXS
D_s	Surface fractal dimension in SAXS

Acknowledgements
The authors are grateful to Ms. Miwako Muro, Mr. Nobuya Morimoto and Dr. Tomoya Imai for performing the experiments, and Ms. Tamaki Morita for thermal modification using ThermoWood®. This work was supported by the Research Institute for Sustainable Humanoshere (RISH), Kyoto University, as a collaborative program for the SAXS analysis. The synchrotron radiation experiments were performed at BL40B2 of SPring-8 with the approval of the Japan Synchrotron Radiation Research Institute (JASRI) (Proposal No. 2021A1192).

Author contributions
MU and TH performed the experiments, and KM analyzed and wrote the manuscript. MN interpreted the data. All authors have read and approved the final manuscript.

Availability of data and materials
The datasets used and/or analyzed during the current study are available from the corresponding author upon reasonable request.

Declarations

Competing interests
The authors declare that they have no competing interests.

Received: 18 March 2023 Accepted: 21 June 2023
Published online: 10 August 2023

References

1. Aytin A, Uygur İ, Demirci T, Akgül İ (2022) The effect of cryogenic treatment on some chemical, physical, and mechanical properties of Thermowood® Oriental spruce. BioResources 17(4):6983–6996. https://doi.org/10.15376/biores.17.4.6983-6996
2. Esteves B, Ayata U, Cruz-Lopes L, Brás I, Ferreira J, Domingos I (2022) Changes in the content and composition of the extractives in thermally modified tropical hardwoods. Maderas Cienc Tecnol 24(22):1–14. https://doi.org/10.4067/s0718-221x2022000100422
3. Kačíková D, Kubovský I, Gaff M, Kačík F (2021) Changes of meranti, padauk, and merbau wood lignin during the ThermoWood process. Polymers 13(7):993. https://doi.org/10.3390/polym13070993
4. Kačík F, Kubovský I, Bouček J, Hrčka R, Gaff M, Kačíková D (2023) Colour and chemical changes of black locust wood during heat treatment. Forests 14(1):73. https://doi.org/10.3390/f14010073
5. Danihelová A, Vidholdová Z, Gergeľ T, Spišiaková Kružlicová LS, Pástor M (2022) Thermal modification of spruce and maple wood for special wood products. Polymers 14(14):2813. https://doi.org/10.3390/polym14142813
6. Torniainen P, Popescu C, Jones D, Scharf A, Sandberg D (2021) Correlation of studies between colour, structure and mechanical properties of commercially produced ThermoWood® treated Norway spruce and scots pine. Forests 12(9):1165. https://doi.org/10.3390/f12091165
7. Pockrandt M, Jebrane M, Cuccui I, Allegretti O, Uetimane E, Terziev N (2018) Industrial Thermowood® and Termovuoto thermal modification of two hardwoods from Mozambique. Holzforschung 72(8):701–709. https://doi.org/10.1515/hf-2017-0153
8. Mitchell PH (1988) Irreversible property changes of small loblolly pine specimens heated in air, nitrogen, or oxygen. Wood Fiber Sci 20(3):320–355
9. Kurenuma Y, Nakano T (2012) Analysis of stress relaxation on the basis of isolated relaxation spectrum for wet wood. J Mater Sci 47(11):4673–4679. https://doi.org/10.1007/s10853-012-6335-0
10. Myose W, Sato T, Kubota M (2020) Numerical calculation of relaxation spectrum based on Fourier transform: Study on viscoelasticity of wood. J Struct Constr Eng (Trans AIJ) 85(773):933–943. https://doi.org/10.3130/aijs.85.933
11. Nakao S, Nakano T (2011) Analysis of molecular dynamics of moist wood components by applying the stretched-exponential function. J Mater Sci 46(14):4748–4755. https://doi.org/10.1007/s10853-011-5385-z
12. Jakob HF, Fengel D, Tschegg SE, Fratzl P (1995) The elementary cellulose fibril in *Picea abies*: Comparison of transmission electron microscopy, small-angle X-ray scattering, and wide-angle X-ray scattering results. Macromolecules 28(26):8782–8787. https://doi.org/10.1021/ma00130a010
13. Hou Z, Fu D, Qin QH (2011) An exponential law for stretching–relaxation properties of bone piezovoltages. Int J Solids Struct 48(3–4):603–610. https://doi.org/10.1016/j.ijsolstr.2010.10.024
14. Sasaki K, Takatsuka M, Kita R, Shinyashiki N, Yagihara S (2018) Enthalpy and dielectric relaxation of poly(vinyl methyl ether). Macromolecules 51(15):5806–5811. https://doi.org/10.1021/acs.macromol.8b00780
15. Aso K (1951) Study on the apparent density of cell wall by the water displacement method. (I). J Jpn For Soc 33(1):19–20. https://doi.org/10.11519/jjfs1934.33.1_19
16. Finnish ThermoWood Association (2003) ThermoWood® Handbook. https://thermalwoodcanada.com/images/PDF/Thermowood_handbook.pdf. Accessed in June 5, 2023

17. Sugino H, Sugimoto H, Miki T, Kanayama K (2007) Fine structure changes of wood during moisture adsorption and desorption process analyzed by X-ray diffraction measurement. Mokuzai Gakkaishi 53(2):82–89. https://doi.org/10.2488/jwrs.53.82
18. Penttilä PA, Rautkari L, Österberg M, Schweins R (2019) Small-angle scattering model for efficient characterization of wood nanostructure and moisture. J Appl Cry 52(2):369–377. https://doi.org/10.1107/S1600576719002012
19. Zhang Y, Inouye H, Yang L, Himmel ME, Tucker M, Makowski L (2015) Breakdown of hierarchical architecture in cellulose during dilute acid pretreatments. Cellulose 22(3):1495–1504. https://doi.org/10.1007/s10570-015-0592-4
20. Dékány I, Turi L, Homonnay Z, Vértes A, Burger K (1996) Preparation of nanosize FeS particles on SiO_2 and clay mineral supports: SAXS and Mössbauer spectroscopic measurements. Colloids Surf A Physicochem Eng Aspects 119(2–3):195–203. https://doi.org/10.1016/S0927-7757(96)03756-9
21. Ufodike CO, Eze VO, Ahmed MF, Oluwalowo A, Park JG, Okoli OI, Wang H (2020) Evaluation of the inter-particle interference of cellulose and lignin in lignocellulosic materials. Int J Biol Macromol 147(15):762–767. https://doi.org/10.1016/j.ijbiomac.2020.01.234
22. Liu Y, Paskevicius M, Sofianos MV, Parkinson G, Li CZ (2021) In situ SAXS studies of the pore development in biochar during gasification. Carbon 172:454–462. https://doi.org/10.1016/j.carbon.2020.10.028
23. Sun B, Wang Z, Liu J (2017) Changes of chemical properties and the water vapour sorption of *Eucalyptus pellita* wood thermally modified in vacuum. J Wood Sci 63:133–139. https://doi.org/10.1007/s10086-016-1601-4
24. Hietala S, Maunu SL, Sundholm FF, Jämsä S, Viitaniemi P (2002) Structure of thermally modified wood studied by liquid state NMR measurements. Holzforschung 56(5):522–528. https://doi.org/10.1515/HF.2002.080
25. Kubovský I, Kačíková D, Kačík F (2020) Structural changes of oak wood main components caused by thermal modification. Polypers 12:485. https://doi.org/10.3390/polym12020485
26. Bhuiyan MR, Hirai N, Sobue N (2000) Changes of crystallinity of wood cellulose by heat treatment under dried and moist conditions. J Wood Sci 46(6):41–436. https://doi.org/10.1007/BF00765800
27. Jakob HF, Tschegg SE, Fratzl P (1996) Hydration dependence of the wood-cell wall structure in *Picea abies*. A small-angle X-ray scattering study. Macromolecules 29(26):8435–8440. https://doi.org/10.1021/ma9605661
28. Penttilä PA, Kioppeläine P, Tolonen L, Suuronen JP, Sixta H, Willför SR (2013) Effects of pressurized hot water extraction on the nanoscale structure of birch sawdust. Cellulose 20(6):2335–2347. https://doi.org/10.1007/s10570-013-0001-9

Publisher's Note

Springer Nature remains neutral with regard to jurisdictional claims in published maps and institutional affiliations.

Submit your manuscript to a SpringerOpen journal and benefit from:

- ► Convenient online submission
- ► Rigorous peer review
- ► Open access: articles freely available online
- ► High visibility within the field
- ► Retaining the copyright to your article

Submit your next manuscript at ► springeropen.com